Impact of EMC Filters on the Power Density of Modern Three-Phase PWM Converters

Marcelo Lobo Heldwein, *Member, IEEE*, and Johann W. Kolar, *Senior Member, IEEE*

***Abstract*—Electromagnetic compatibility (EMC) filters are typically included in offline power converters, controlling electromagnetic emissions, but adding volume to power electronic systems. During the last decades, one of the main objectives of the power electronics industry has been the increase of the power density. Thus, it is reasonable to analyze how filters affect power density values, imposing limits or "barriers" to it. The impact of the EMC filters on the overall volume of three-phase pulsewidth modulation (PWM) converters is studied here for converters in the range of 5–10 kW. An analytical procedure based on the volume minimization of the EMC filters is proposed to estimate the total filter volume as function of the converters' rated power and switching frequency. With this, the minimum volume for EMC filters that allow the converters to comply with EMC standards regarding conducted emissions can be estimated and volume limitations identified. A discussion about the limits of power density for the considered three-phase PWM converters for state-of-the-art power semiconductors is performed, and optimum switching frequencies are identified. An experimental verification is carried out, which validates the achieved results.**

***Index Terms*—Electromagnetic compatibility (EMC) filters, power density, sparse matrix converter (SMC), three-phase pulsewidth modulation (PWM) converters, Vienna rectifier.**

I. Introduction

POWER electronics three-phase converters are used in the many different types of industry to supply stable and reliable dc or ac energy to equipment, motors, and batteries. These converters typically exhibit a few very important characteristics, namely: 1) high-power conversion efficiency, 2) small volume, 3) high reliability, 4) safety to the users, and 5) electromagnetic compatibility. High efficiency and small volume are commons aims among end users and manufacturers, while the other characteristics can be seen as end user requirements. Some of these characteristics have been translated into national and international standards that set minimum requirements for the different types of equipment.

In order to address the evolution of pulsewidth modulation (PWM) converters, different figures of merit (FOM) can be employed. PWM converters are typically rated for the power that they are able to supply, their "rated power." Thus, an appropriate quantity, as suggested in [1] and [2], is the power density of the converters, which is defined as the ratio between rated output power P_o and volume Vol of the system Vol, $\rho = P_o/\text{Vol}$.

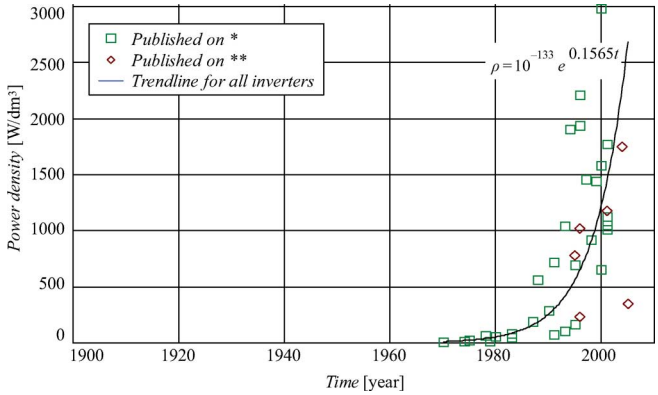

Fig. 1. Change in power density for inverters as published in [1]–[3]. An exponential trend line based on the measured points is shown.

Two classes of equipment are considered here, inverters and rectifiers. In Fig. 1, the power density evolution for inverters is shown. These results have been published in [1]–[3], and show that an exponential growth is seen since the early 1970's. This has been enabled by the use of high-frequency PWM converters, which make use of ever-improving power semiconductors. It is also observed in [1] and [2] that the continuous improvement of semiconductor technology must endure if this exponential growth is to be continued.

Rectifiers with various power ratings are observed in practice. However, considering all power ranges and applications would require a large classification effort. For this reason, only rectifiers ranging from 1 to 100 kW are considered here. Furthermore, high-power rectifiers are a good measure for the whole field since they are equipment with high aggregated value. Special focus is placed on dc power supplies for telecommunication systems, which demand high performance due to stringent standards in the field. The collection of data has been acquired from books, magazines, scientific journals, manufacturers' homepages, product catalogs, articles published in the World Wide Web, and personal communication (e-mail) with industry personnel. The collected data for these rectifiers are presented in Fig. 2 for the different switch technologies. Transistors were invented in the late 1950's and 1960's, but were incorporated in products ten to 20 years later. It is seen that much less progress is observed until the 1990's, when high research efforts were applied in order to achieve better circuits, switches, magnetic materials, and capacitors, besides the employment of digital processors [4]. For this reason, two

Manuscript received December 11, 2008. Current version published June 10, 2009. Recommended for publication by Associate Editor P. Tenti.

M. L. Heldwein is with the Power Electronics Institute (INEP), Federal University of Santa Catarina, Florianópolis 88040-970, Brazil (e-mail: heldwein@inep.ufsc.br).

J. W. Kolar is with the Power Electronic Systems Laboratory, Swiss Federal Institute of Technology (ETH) Zurich, Zurich CH-8092, Switzerland (e-mail: kolar@lem.ee.ethz.ch).

Color versions of one or more of the figures in this paper are available online at http://ieeexplore.ieee.org.

Digital Object Identifier 10.1109/TPEL.2009.2014238

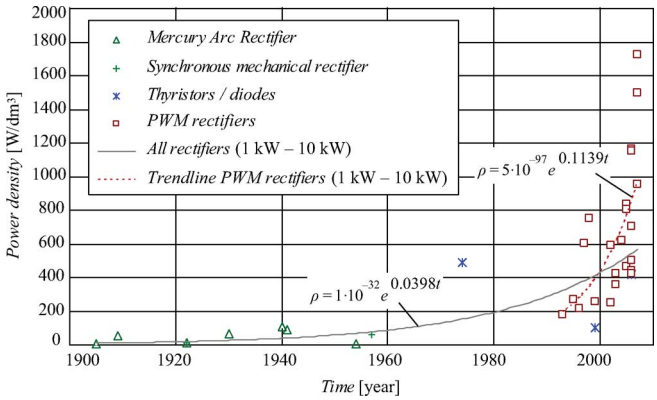

Fig. 2. Evolution of power density over time for power rectifiers rated from 1 up to 100 kW. Two exponentially fitted curves are shown: one for all (full line) collected points and another for the lately introduced high-frequency switched-mode power rectifiers (dashed).

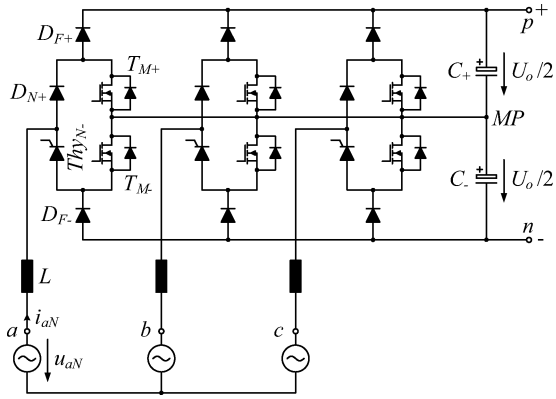

Fig. 3. Circuit schematic of a three-phase, six-switch, three-level boost-type rectifier [13].

tendency curves are shown in Fig. 2; one shows the exponential fitted curve for the complete data set and the other that approximates the rapid growth observed on the high-frequency PWM converters. The use of high switching frequencies has enabled the reduction of passive components volume, and is the main factor for the current exponential increase in the power density. Research-oriented prototypes are typically preceding products from five to ten years [1], [2], and based on these, it is expected that the exponential growth in power density for this class of rectifiers continues. However, it is very difficult to predict for how long since it depends on a number of different enabling technologies, such as materials, circuits, and scientific understanding.

Two of the main factors that influence the power density of power converters are the cooling system and the passive components, where the electromagnetic compatibility (EMC) filters are responsible for a substantial part [5], [6]. Increase in the power density is possible, in principle, with an increase of switching frequency or the operating temperature of the power semiconductors. Higher switching frequencies (smaller passive components), however, lead to higher switching losses (larger cooling systems). Therefore, a compromise exists, in which a power electronics engineer must work and find an optimum.

A timely necessity to address the impact, from the perspective of limiting power density, of the filters for the discussed modern three-phase PWM converter systems has, thus, motivated this study. In order to achieve this objective, two topologies are chosen, namely: a three-phase ac–dc–ac sparse matrix converter (SMC) and a three-phase power factor correction (PFC) Vienna rectifier. The design of the EMC filters for these topologies is performed in order to obtain minimum volume filters based on the presented filter design practices. The calculated filters present a minimum limitation for the achievable power density of the power converters, and consequently, are of high importance during the design of power converters. This procedure is presented in the following sections, starting in Section III with the dimensioning of the filter components, explaining the filter design procedure (cf., Section IV) for both converters, and presenting the obtained results and comparing them with built prototypes in Sections V and VI.

II. Modern Three-Phase PWM Converters

Even presenting power and control circuits that are typically more complex than other alternatives [7], [8], three-phase PWM converters have increased their share in the market due to clear advantages [7]–[11], such as: 1) very high efficiency, 2) robustness to mains transients, 3) high-power factor, 4) wide range of output frequencies, 5) small dimensions, 6) ride-through capability, 7) regeneration, 8) ease of implementing protection circuits, and 9) excellent control features. On the other hand, PWM converters present some side effects mainly due to the pulsed waveforms with rich spectral contents and very fast transient times [12]. Thus, they typically require input filters to comply with EMC requirements.

Three-level boost-type rectifiers (cf., Fig. 3) have been proposed in the literature [13], [14] for more than a decade, and there are already several applications into commercially available equipment [15], and find increasing interest due to the following advantages: possibility of employing switches with reduced rated voltages, thus, lowering switching losses and increasing efficiency, reduced input inductor due to the lower voltage steps applied to these inductors, and high controllability of the input currents. Nevertheless, these converters present high common mode voltages, which shall be properly attenuated for achieving EMC.

Regarding inverter systems, even though the voltage source inverter (VSI) is the most broadly employed converter, modern matrix converter topologies are believed to achieve higher power densities, and therefore, are considered here instead of back-to-back systems. Matrix converters have already been integrated into commercial products [16]; however, they have not received much attention in the research of EMC. Indirect [13], [17] and SMCs [18]–[22], as seen in Fig. 4, have been broadly researched in the last years due to their capability of simultaneously providing three-phase voltage amplitude and frequency transformation, achieving high efficiencies and small overall volumes [7].

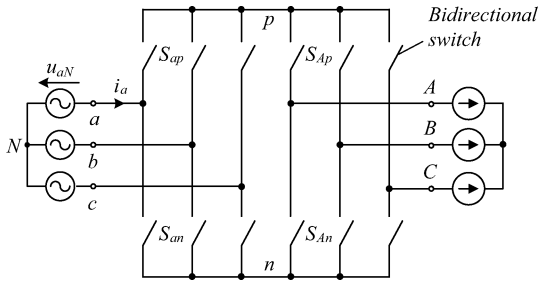

Fig. 4. Circuit schematics of three-phase indirect and SMC topologies.

Nevertheless, very few technical papers have specifically addressed the challenges from an EMC perspective.

III. Volume Estimation of Filter Components

In order to evaluate the impact of EMC filters on the power density of three-phase PWM converters, the volume of the employed filtering components must be known. For analyzing the maximum achievable power density figures, the volume of such components must be the smallest possible. Thus, this section discusses the design of the filter components assuming necessary simplifications, so that the volume of the components can be predicted beforehand and the achieved volume is close to the smallest possible with today's commercially available materials and components.

A. Volume Estimation for Common Mode Inductors

To estimate the volume of common mode (CM) inductors, a series of inductor designs is conducted for different ripple frequencies and current ratings. This procedure is performed in order to evaluate how volume and achievable impedance depend on design parameters such as maximum temperature rise, ripple frequency, and rated current. The design procedure is based on the following assumptions:

1) possible asymmetries, parasitic capacitances, and the effect of the tolerances are neglected;
2) ambient temperature equals 45 °C, and the maximum temperature rise is 75 °C;
3) a single winding layer is allowed in order to reduce parasitics;
4) iterative choice of the maximum flux density $B_{\max}$ and current density $J_{\max}$ is performed;
5) discrete values determined by the limited choice of cores and wire diameters are approximated by continuous functions.

For the design of the CM choke, a maximum window factor of 0.28 is considered. The design takes into consideration the variation of the complex permeability of the cores as well as the total losses. In order to simplify the analysis, only material VITROPERM 500 F is considered here. Furthermore, only the cores commercially available from Vacuumschmelze (VAC) [23], [24] are employed, leading to ten different sizes of inductor (cf., Fig. 5).

In Fig. 5, the dependency of the volume of an inductor to its product of areas $A_e A_w$ is depicted along with the core volume

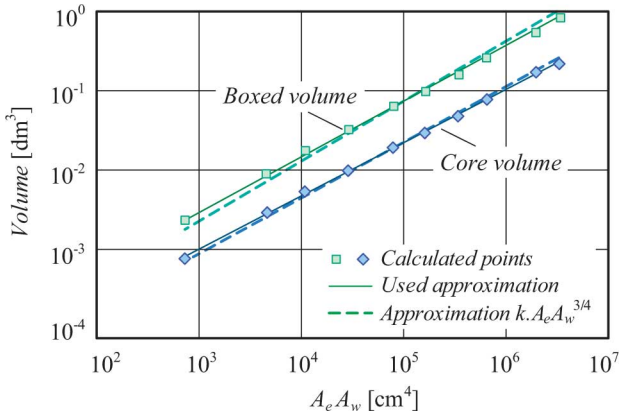

Fig. 5. Dependency of an inductor's boxed and core volume on area product $A_e A_w$ of the used material.

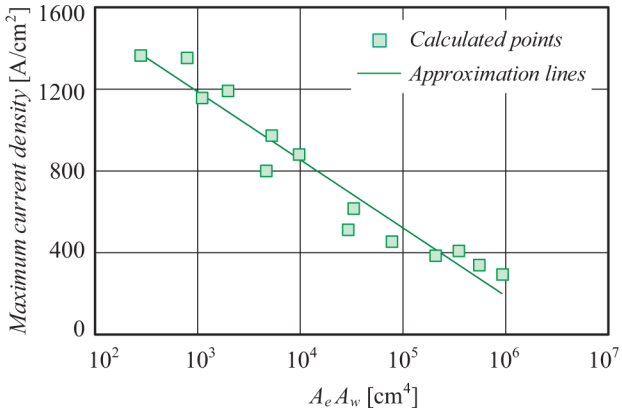

Fig. 6. Maximum current density as a function of the area product.

for two types of core coatings, namely epoxy-coated cores and cores with a plastic enclosure. This dependency is usually considered with a power of $3/4$, but for the case at hand, a lower factor is employed leading to closer approximations. With this, the volume of the filter inductor $\mathrm{Vol}_{L\,CM}$ is calculated with

$$\mathrm{Vol}_{L\,CM} = k_{\mathrm{geo}} (A_e A_w)^{\alpha_{\mathrm{geo}}} \tag{1}$$

with $k_{\mathrm{geo}} \cong 10.776 \times 10^{-2}$ [dm^3] and $\alpha_{\mathrm{geo}} \cong 0.7052$ for the cores with a plastic enclosure.

From the results obtained in the performed designs, approximative functions are empirically derived for the maximum current density $J_{\max}$ and the maximum flux density $B_{\max}$ as functions of the core product of areas $A_e A_w$ and switching frequency f_s, respectively.

The maximum current density $J_{\max}$ curve is presented in Fig. 6. Since the relation between the outer surface and the volume of the toroidal inductors is more favorable for small cores, larger inductors require lower current density.

The maximum flux density $B_{\max}$ is plotted in Fig. 7. It is observed that the employed maximum flux density is a fraction of the saturation flux B_{sat} for low switching frequencies, but as it increases, the flux density is reduced, and thus, keeps core losses under controlled values. The core losses are simply computed with the peak harmonic at the switching frequency and using

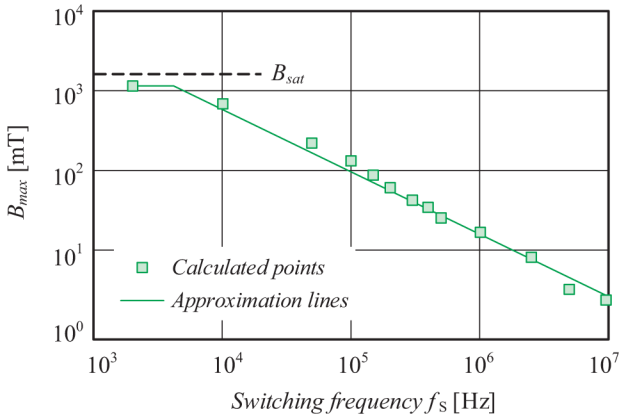

Fig. 7. Maximum flux density as a function of the switching frequency.

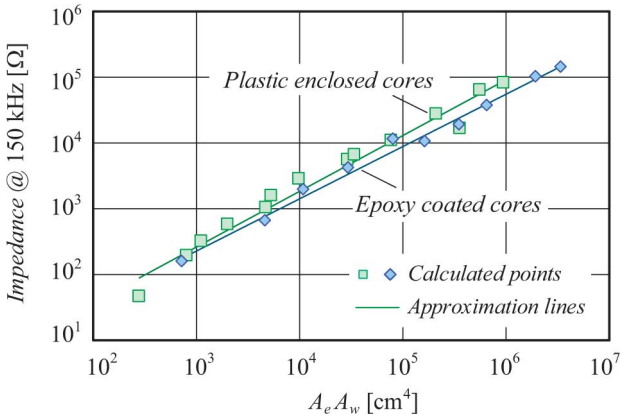

Fig. 8. Impedance at $f_{\rm int} = 150$ kHz and 15 A (rms) as a function of area product for two core types namely, epoxy-coated cores and cores with a plastic enclosure employing VITROPERM 500 F.

the Steinmetz equation. This simplification is necessary in order to achieve a time efficient algorithm for the volume calculation. In a precise design, this would have to be specially considered if the switching frequency is very high ($\gg$100 kHz). The core losses are designed to be lower than 20% of the total losses.

Considering the commercially available discrete cores and computing the maximum impedance that each of them is capable of providing at each specified design point leads to the information on the smallest inductor volume for a given impedance. Finally, based on these considerations and on the material's complex permeability $\mu(f)$, an equation for the achievable CM impedance Z_{CM} for a given product of areas and switching frequency is empirically derived

$$Z_{CM}(f_{\rm int}) \cong 10^{2.243-2\log(I_N)+0.181\log(|\mu(f_{\rm int})|f_{\rm int})\log(A_e A_w)} \tag{2}$$

where I_N is the inductor's rms current and $f_{\rm int}$ is the frequency of interest. As an example, Fig. 8 shows the calculated impedance at $f_{\rm int} = 150$ kHz and $I_{N1} = 15$ A as a function of area product for two core types.

Equation (2) presents an R-squared value higher than 0.939 for frequencies in the range 150 kHz $\leq f_{\rm int} \leq$ 10 MHz, when compared with the calculated values. Solving (2) for the product of areas leads to the core size, and its volume can be calculated with the help of (1).

B. Volume Estimation of Differential Mode (DM) Inductors

The design of the DM inductors is considerably different than that of CM ones. The DM currents are composed of a high mains frequency component and a relatively small high-frequency ripple due to the attenuation given by the input inductors and/or capacitors $C_{DM,1}$. Thus, the cross-sectional area of the core A_e is determined mainly by saturation and not by core losses. Furthermore, the high-frequency losses in the winding are also comparatively small and can be neglected. The other parameter that defines the core is the required winding area A_w. The filter inductance L_{DM} and rated current are related to the size of the required core area product by

$$L_{DM}\, I_{N,\rm peak}\, I_N = k_w\, J_{\rm max} B_{\rm peak} A_e A_w \tag{3}$$

where k_w is the window occupation factor.

The volume of the filter inductor $\mathrm{Vol}_{L_{DM}}$ is calculated with

$$\mathrm{Vol}_{L_{DM}} = k_{\rm geo}(A_e A_w)^{\alpha_{\rm geo}} \tag{4}$$

where, the parameters $k_{\rm geo}$ and $\alpha_{\rm geo}$ account for the geometry of the core (toroidal, planar, etc.). Assuming that a dimension grows proportionally with the other ones, $\alpha_{\rm geo}$ is typically taken as 3/4.

With the implementation of an iterative procedure for designing DM inductors, a series of designs performed in a computer is a simple task. Therefore, in order to evaluate the volume of DM inductors, a series of designs have been performed with the following specifications:

1) ambient temperature: $T_{\rm amb} = 45\,^\circ$C;
2) maximum temperature: $T_{\rm max} = 100\,^\circ$C;
3) maximum current: $I_N = 0.5, \ldots, 20$ A (equally divided in ten points);
4) frequency of interest: $f_{\rm int} = 150$ kHz;
5) desired inductance at $f_{\rm int}$: $L_{\rm des} = 1, \ldots, 200\,\mu$H (equally divided in ten points).

Thus, a total of 10×10 designs have been performed per core material. In these designs, core losses have been neglected in order to obtain the dependency of the inductors' smallest possible volume on the rated current and required inductance at 150 kHz. From the computed volume for each of the designed inductors, a linear regression through least squares has been performed in order to fit the function

$$\mathrm{Vol}_L = k_L \frac{1}{2} L\, I_N^2 \tag{5}$$

to the obtained results. As an example, material high flux with $\mu_r = 60$ has been chosen, and the design results for this material are presented in Fig. 9. A good agreement is observed between the fitted function with $k_L = 3.95 \times 10^{-3}$ dm^3/J and the design points, validating the choice for this type of function.

The final values computed for the considered magnetic materials are presented in Fig. 10, where it is seen that only four materials have volumetric coefficients lower than 5 dm^3/J, namely: molybdenum permalloy powder (MPP) with $\mu_r = 60$ and high

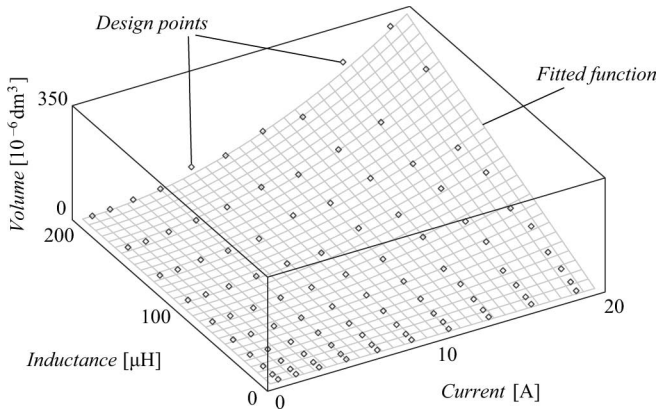

Fig. 9. Computed volume compared with the fitting function for material high flux with $\mu_r = 60$.

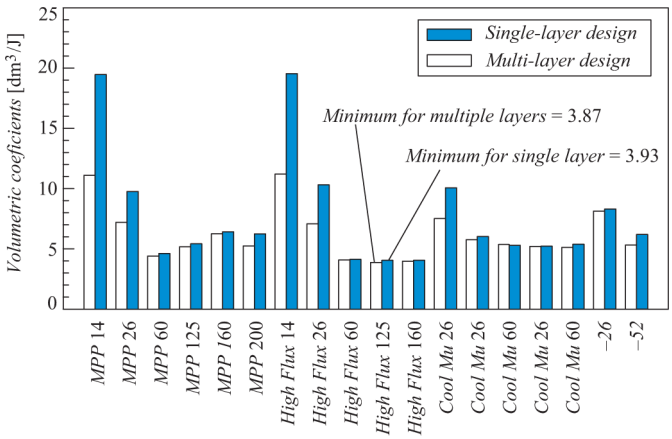

Fig. 10. Computed volumetric coefficients for DM inductors employing the listed materials.

flux with $\mu_r = 60, 125$, and 160. The lower permeability materials are preferred since the variation of permeability with dc bias is reduced. For these reasons, materials MPP and high flux, both with $\mu_r = 60$, are recommended for DM filter inductors of compact size. MPP has the advantages of lower core losses and higher thermal limits. Nevertheless, high flux is less costly and leads to smaller inductors, thus, being generally preferred.

C. Volume Estimation of Filter Capacitors

1) CM Capacitors: Equipment safety regulations play an important role in filter design, hence limit the maximum values for earth leakage currents, define requirements for capacitors between an input line and protective earth (PE), and define insulation requirements for CM inductors and filter construction. Earth leakage current $I_{\mathrm{PE,rms,max}}$ is typically limited to 3.5 mA, even for the case where one of the phases is lost. Thus, the total capacitance $C_{CM,\mathrm{sum}} = \sum C_{CM,i}$, (where $i = 1, \ldots, 3$), between any of the input phases and the PE is bounded to a maximum that depends on the rated voltage U_N by

$$C_{CM,\mathrm{sum}} \leq \frac{I_{\mathrm{PE,rms,max}}}{1.1 \times U_{N,\mathrm{max}} \times 2\pi \times 50\,\mathrm{Hz}} \cong 44\ \mathrm{nF}. \quad (6)$$

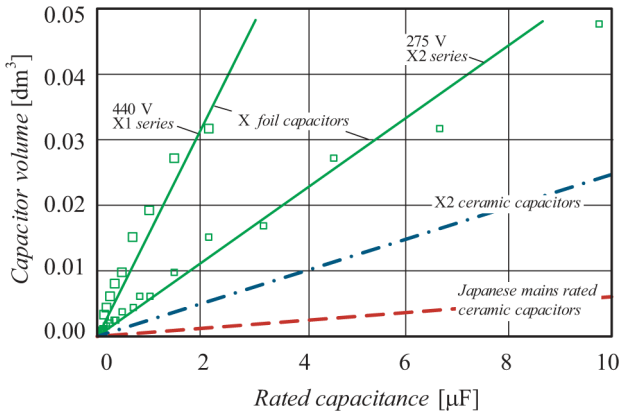

Fig. 11. Volume and approximation curves for mains rated capacitors.

TABLE I
VOLUMETRIC COEFFICIENT FOR DIFFERENT X CAPACITORS TECHNOLOGIES

Technology	*Manufacturer*	*Voltage*	k_C
X2 foil	Evox-Rifa	275 V / 400 V	$46.9 \cdot 10^{-6}\ \frac{\mathrm{m}^3}{\mathrm{F \cdot V}^2}$
X2 ceramic	Murata	250 V	$16.4 \cdot 10^{-6}\ \frac{\mathrm{m}^3}{\mathrm{F \cdot V}^2}$
Jap. mains cer.	Murata	250 V	$4.07 \cdot 10^{-6}\ \frac{\mathrm{m}^3}{\mathrm{F \cdot V}^2}$

This is a very low value and ensures that, for minimum volume CM filters, the maximum amount of capacitors from phase to PE must be employed. Safety requires Y2-rated capacitors for connections between phase and PE. Due to these restrictions, a series of Y2 ceramic capacitors [25] is chosen, which presents a maximum capacitance of 4.7 nF per SMD package, leading to compact construction and low parasitics. The volume of each SMD unit of this series is approximately $\mathrm{Vol}_{C_{CM},\mathrm{unit}} \cong 52 \times 10^{-9}\ \mathrm{m}^3$. Since other capacitances are present in the circuit (arrestors, stray capacitances, etc.) and values present tolerances, some margin is provided so that $C_{CM,\mathrm{sum}} = 8 \times 4.7\ \mathrm{nF} = 37.6\ \mathrm{nF}$, to be divided in the three CM filter stages. It can be proved [26] that, for maximum attenuation given a minimum total capacitance, each stage shall present the same value. With this, $C_{CM,i} = C_{CM,\mathrm{sum}}/3$.

2) DM Capacitors: Assuming that the volume of the components is directly related to their stored energy, the volume of DM capacitors is defined as

$$\mathrm{Vol}_{C,i} = k_C C_{DM,i} U_N^2. \quad (7)$$

The coefficients k_C are obtained by minimum squares regression of the volumes calculated for commercially available X-type capacitors (foil [27] and ceramics [25]) as well as for ceramic capacitors rated for the Japanese mains [25]. These are plotted in Fig. 11 along with approximation curves. The calculated volumetric coefficients are given in Table I. A very high smaller volumetric coefficient is observed for the ceramic type of capacitors, allowing for more compact filters.

IV. DESIGN PROCEDURE FOR THE EMC FILTERS

The power converter topologies, which are considered for this study, are presented in Figs. 12 and 13. These topologies are

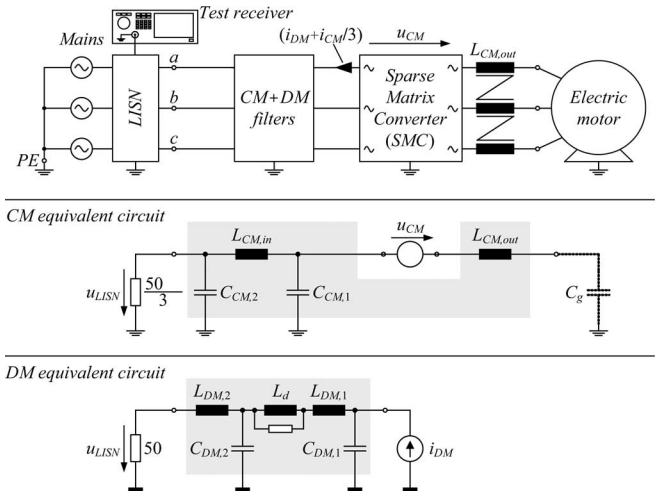

Fig. 12. Considered converter, filter topologies, and simplified equivalent circuits for an SMC.

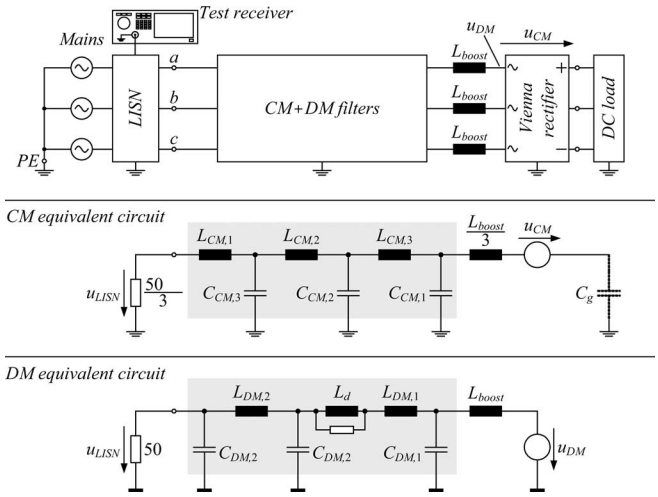

Fig. 13. Considered converter, filter topologies, and simplified equivalent circuits for a Vienna Rectifier.

shown as simplified equivalent circuits used for the filter design calculations. A further simplification is that the line impedance stabilization network (LISN) circuits are replaced with 50 Ω resistors modeling the input resistance of an EMC test receiver. It is shown in Fig. 12 that two-stage filters are considered for an SMC, and in Fig. 13 three-stage filters are considered for the Vienna rectifier. For the SMC, an output CM choke is included, since the CM voltage at the input terminals of the electric motor must be limited [28]. The output cable and the machine typically present a high capacitance value to PE when compared to the capacitance between semiconductors and cooling system. Therefore, for simplicity reasons, this is the only capacitance considered for the SMC filters. The first DM capacitors $C_{DM,1}$ are chosen in order to limit the high frequency ripple at the input voltages of the SMC to $\pm 7.5\%$ of the peak input rms voltage. For the Vienna rectifier, the boost inductors L_{boost} are also considered as part of the filters, although their design is done based on the limitation of the input current ripple to 10% of the peak current, and the used materials are high-performance ferrites.

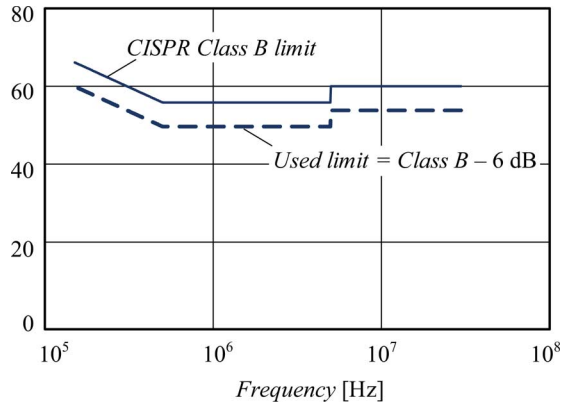

Fig. 14. Conducted emissions limit used in this study equals the CISPR class B minus 6 dB.

The starting point for the filter design is the estimation of the frequency spectrum for DM voltages and currents and CM voltages, which is compared to the desired limits at the frequency of interest f_{int}, which is 150 kHz for switching frequencies lower than 150 kHz or the switching frequency for higher frequencies. This leads to a required attenuation $\mathrm{Att}_{\mathrm{req}}$ at the frequency of interest.

The design is based on the calculation of filter components values that lead to minimum volume filters, which fulfill conducted emissions (CEs) requirements for CISPR 11 [29] Class B equipment in the frequency range of 150 kHz–30 MHz. The limits taken into consideration for all designs performed here is actually 6 dB lower, as displayed in Fig. 14. A series of simplifications is assumed in order to keep a reasonable calculation effort, which are as follows.

1) The accurate calculation of the harmonic contents of the switched voltages of the power converters is replaced by simplified envelopes, functions of topology, modulation index, and switching frequency, which do not consider the influence of parasitics, and rise and fall times.
2) All three-phase circuits are considered symmetric, so that single-phase equivalents are used.
3) The parasitics, intercomponent couplings, and the effects of the tolerances of the designed filter components are neglected for attenuation calculation.
4) Parasitics in the power converters are neglected, except for all capacitances to PE, which are responsible for CM paths and are lumped into one capacitance C_g.
5) Effects of internal power supplies and gate drive circuits are neglected.
6) The discrete values of components and core dimensions are linearized.

The empirically derived expressions for the envelope functions for the SMC are given by

$$\varsigma_{i_{DM,\mathrm{SMC}}}(f) = \begin{cases} \frac{1}{2\sqrt{2}} \left| \frac{I_{2,\mathrm{peak}}\, M}{1 + j\,\pi\, M\, \frac{f}{f_s}} \right|, & \text{if } f \le f_s \\ \frac{1}{2} \left| \frac{I_{2,\mathrm{peak}}\, M}{1 + j\,\pi\, M\, \frac{f}{f_s}} \right|, & \text{if } f_s < f \le 6 f_s \\ \frac{1}{2\sqrt{2}} \left| \frac{I_{2,\mathrm{peak}}\, M}{1 + j\,\pi\, M\, \frac{f}{f_s}} \right|, & \text{if } 6 f_s < f \end{cases} \quad (8)$$

for the DM equivalent current source and by

$$\varsigma_{u\,CM,\mathrm{SMC}}(f)=\begin{cases}\frac{1}{\sqrt{6}}\left|\frac{U_{N1}\,M}{1+j\,\pi\,M\frac{f}{f_s}}\right|, & \text{if } f\le f_s\\ \frac{2}{\sqrt{6}}\left|\frac{U_{N1}\,M}{1+j\,\pi\,M\frac{f}{f_s}}\right|, & \text{if } f_s<f\le 6f_s\\ \frac{1}{\sqrt{6}}\left|\frac{U_{N1}\,M}{1+j\,\pi\,M\frac{f}{f_s}}\right|, & \text{if } 6f_s<f\end{cases}\quad(9)$$

for the CM equivalent voltage source.

The envelope functions for the Vienna rectifier are defined by

$$\varsigma_{u\,DM,\mathrm{VR}}(f)=\begin{cases}\left|\frac{U_o\,M}{1+j\,\pi\,M\frac{f}{f_s}}\right|, & \text{if } f\le f_s\\ \frac{2}{\sqrt{6}}\left|\frac{U_o\,M}{1+j\,\pi\,M\frac{f}{f_s}}\right|, & \text{if } f_s<f\le 6f_s\\ \frac{1}{\sqrt{6}}\left|\frac{I_{2,\mathrm{peak}}\,M}{1+j\,\pi\,M\frac{f}{f_s}}\right|, & \text{if } 6f_s<f\end{cases}\quad(10)$$

for the DM equivalent voltage source and by

$$\varsigma_{u\,CM,\mathrm{VR}}(f)=\begin{cases}2\sqrt{2}\left|\frac{U_o\,M}{1+j\,\pi\,M\frac{f}{f_s}}\right|, & \text{if } f\le f_s\\ 4\sqrt{2}\left|\frac{U_o\,M}{1+j\,\pi\,M\frac{f}{f_s}}\right|, & \text{if } f_s<f\le 6f_s\\ \frac{3}{\sqrt{2}}\left|\frac{U_o\,M}{1+j\,\pi\,M\frac{f}{f_s}}\right|, & \text{if } 6f_s<f\end{cases}\quad(11)$$

for the CM equivalent voltage source.

A. DM Filter Design

In order to guarantee that the designed filters are of minimal volume, the desired component values can be derived as functions of two equations, namely the required attenuation at a given frequency and the total volume, which is to be minimized. The main assumptions assumed here are: 1) the inductors are designed for their low-frequency rms current, 2) the parasitics of the components do not influence the attenuation at the relevant frequency, and 3) the boost inductor is not included in the analysis and has its value defined by current ripple requirements. In order to simplify the problem, the asymptotic approximation of the attenuation Att for an *LC* filter is used, which leads to an equation of this type

$$\mathrm{Att}(\omega)=\frac{1}{\omega^{2N}\prod_{j=1}^{N}L_j\prod_{j=1}^{N}C_j}.\quad(12)$$

In order to obtain the maximum attenuation for a total inductance, it can be proven that each of the individual inductors must have the same value, and the same is valid for the capacitors. Thus, only two variables are left to minimize the volume. Considering the case of a single *LC* stage, which shows the basic principle of minimizing a filter's volume, the required attenuation $\mathrm{Att}_{\mathrm{req}}$ equation simplifies to

$$\mathrm{Att}_{\mathrm{req}}=\frac{k_{\mathrm{att}}}{L\,C}\quad(13)$$

where, $k_{\mathrm{att}}=1/\omega^2$.

The second equation for the minimization problem is the total volume of the filter $\mathrm{Vol}_{\mathrm{filt}}=\mathrm{Vol}_L+\mathrm{Vol}_C$. It can be assumed that the volume of the components is directly related to their stored energy, so that volumetric coefficients for inductors k_L and capacitors k_C are employed. Thus

$$\mathrm{Vol}_{\mathrm{filt}}=k_L\,L\,I_N^2+k_C\,C\,U_N^2.\quad(14)$$

Isolating L leads to

$$\mathrm{Vol}_{\mathrm{filt}}=k_L\,L\,I_N^2+k_C\,\frac{k_{\mathrm{att}}}{L\,\mathrm{Att}_{\mathrm{req}}}\,U_N^2.\quad(15)$$

By differentiating (15) with respect to L, the minimum volume point is found with the components defined by

$$L=\frac{U_N}{\omega I_N}\sqrt{\frac{k_C}{k_L\,\mathrm{Att}_{\mathrm{req}}}}\quad(16)$$

$$C=\frac{I_N}{\omega U_N}\sqrt{\frac{k_L}{k_C\,\mathrm{Att}_{\mathrm{req}}}}.\quad(17)$$

The same procedure can be extended to multistage filters. Thus, minimal volume filters can be designed based on the ratings of the components and their volumetric coefficients.

Requirements related to control issues must be considered. In order to provide sufficient passive damping causing minimum losses and avoiding oscillations, also for no-load operation, *RL* networks are included in the choice of the topologies. These networks are used for damping resonant frequencies introduced by the filter components and the uncertainties in the mains impedance, which could shift given resonances or introduce novel resonant circuits with low damping. For simplicity reasons, the influence of the *RL* damping networks in the attenuation is neglected and the inductors L_d are considered to have the same volume as inductors $L_{DM,1}$.

B. CM Filter Design

For the design of the CM filters, the converters are considered as voltage sources u_{CM}, dependent on modulation, input and output voltages, and switching frequencies. The CM filter of the SMC is split into an output CM choke and a two-stage CM filter at the input. The aim of the output choke is to keep the CM rms voltage at the input terminals of the motor lower than 15 V for any switching frequency and capacitances to ground C_g. The remaining components are responsible for providing the total required attenuation.

Two types of components are considered for the CM filters: ceramic capacitors, which are Y2-rated [25], and CM chokes, which are designed based on toroidal nanocrystalline cores VITROPERM 500F [24], and are "state-of-the-art" in their classes. An earth leakage current limitation of 3.5 mA is considered, and this bounds the total capacitance per phase to approximately 40 nF at 50 Hz, which is reduced to 30 nF per phase and evenly distributed among the filter stages.

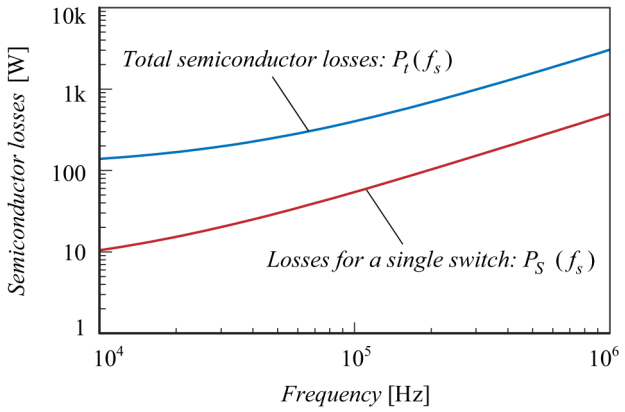

Fig. 15. Calculated semiconductor losses for a 5 kVA IMC with SiC JFETs.

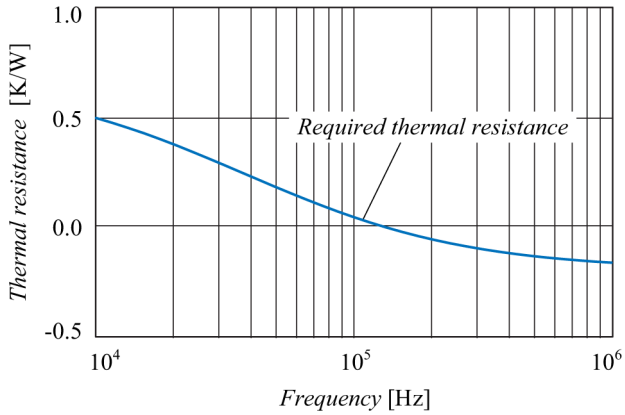

Fig. 16. Maximum thermal resistance required for the cooling system for the SiC-JFET-based IMC.

V. SMC Power Density Limits

With the given volume minimization procedures for CM and DM filters, the impact of the filter volume in the achievable power density is a function of the switching frequency.

An indirect matrix converter topology is assumed, where the power semiconductors are considered to be formed by four SiC JFETs rated for 1200 V, 6 A, and having a channel resistance of 0.5 Ω. These are considered in order to reduce switching losses to the minimum allowed with state-of-the-art semiconductors [30]. The calculated power losses as a function of switching frequency are shown in Fig. 15.

The total losses and the thermal limits for the SiC JFETs define a required thermal resistance for the cooling system. This is computed here with the total thermal resistance between the heat sink and the ambient $R_{\mathrm{th,sa}}$

$$R_{\mathrm{th,sa}}(f_s) \leq \frac{T_j - T_a}{P_t(f_s)} - \frac{P_S(f_s)\, R_{\mathrm{th,jc}}}{P_t(f_s)} - R_{\mathrm{th,cs}} \qquad (18)$$

where T_j is the maximum allowable junction temperature, T_a is the ambient temperature, $R_{\mathrm{th,jc}}$ is the thermal resistance between junction and case for the paralleled JFETs, and $R_{\mathrm{th,cs}}$ is the thermal resistance between the JFETs' case and the heat sink. The parameters adopted in this calculation are $T_j = 125\,^{\circ}\mathrm{C}$, $T_a = 45\,^{\circ}\mathrm{C}$, and $R_{\mathrm{th,jc}} = 1.2$ K/W. The thermal resistance between the semiconductors and the heat sink is neglected, i.e., $R_{\mathrm{th,cs}} = 0$ K/W. The required thermal resistance is estimated as in Fig. 16.

Fig. 16 shows that switching frequencies higher than approximately 120 kHz are not practical for the given set of semiconductors, since negative thermal resistances are required. Active cooling would have to be employed for this condition. From the required thermal resistance, it is possible to estimate the volume for an optimized forced air cooling systems based on [31]. For the calculations, a coefficient CSPI $= 25$ W/K^{-1}liter^{-1} [31] is used, leading to a total volume of the cooling system $\mathrm{Vol}_{\mathrm{hs}}$ given by

$$\mathrm{Vol}_{\mathrm{hs}}(f_s) \geq \frac{1}{\mathrm{CSPI} R_{\mathrm{th,sa}}(f_s)}. \qquad (19)$$

The volume of the various filter components can be derived as functions of the converter ratings, switching frequency, and total capacitance to ground C_g. This is of high importance since optimum switching frequencies can be chosen minimizing the total converter volume.

The design of the input CM inductor is dependent on the output CM inductor as well. It is considered here that the output CM inductor keeps the CM voltage across the load machine below $U_{\mathrm{out,max}} = 15$ V rms. With this, the required impedance for the output CM inductor can be estimated with

$$Z_{L_{CM},\mathrm{out}}(f_s) \geq \frac{U_p(f_s)}{2\,\pi\, f_s\, C_g\, U_{\mathrm{out,max}}} \qquad (20)$$

where $U_p(f_s)$ is the peak voltage of the first harmonic at the switching frequency.

The input CM inductor can have its required impedance estimated based on the required attenuation to achieve compliance with CISPR 11 Class B limits. This leads to an inductor with the volume presented in Fig. 17, where two regions are highlighted. In the first region, the inductor is designed according to the required impedance only and this leads to a fast decrease characteristic ($\cong -20$ dB/decade) regarding higher switching frequencies and the increase of the output inductor impedance. Whereas, in the second region, the volume of the inductor is defined by the maximum flux density allowed in order to keep core losses under control. It is seen that in the second region, the volume of the inductor presents a slower reduction of the volume with increasing switching frequency and output inductor impedance. This characteristic prevents a large reduction in the volume of the components of CM filters with frequency, and identifies that the performance of the state-of-the-art core materials for CM inductors must improve if higher switching frequencies are to be employed in three-phase PWM converters.

The total volume of the components of the EMC filters for a 5-kVA indirect matrix converter is displayed in Fig. 18 along with the contributions of the DM and CM filter volumes as well as the volume of the first DM capacitors $C_{DM,1}$ for a specific value of capacitance to ground of $C_g = 20$ nF. The volume of an optimized cooling system is also included. The DM filters dominate the filters volume for lower switching frequencies. The CM filters volume is highly dependent on the capacitance to ground. The increased volume of the CM filter for low switching

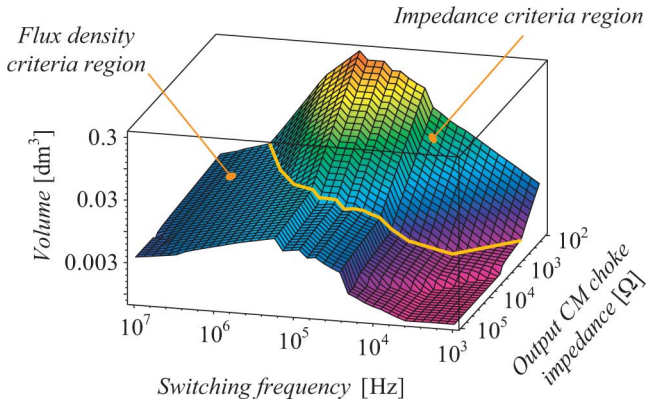

Fig. 17. Volume of the input CM inductor $L_{CM,1}$ as a function of the achievable choke impedance and CM current ripple frequency.

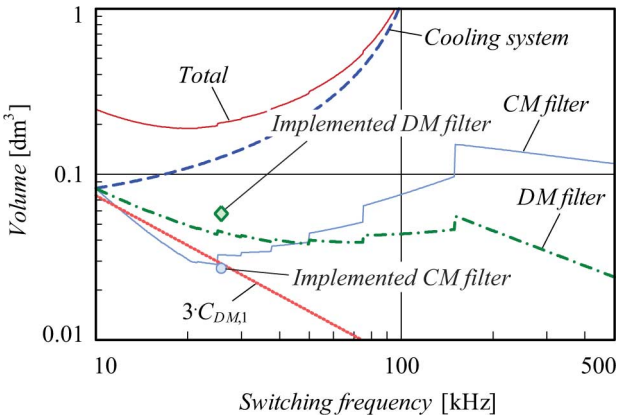

Fig. 18. Total and partial volumes of the EMC filters for an IMC rated for 230 V rms phase voltage, modulation index $M = 0.7$, mains frequency 50 Hz, output power $S_2 = 5$ kVA, and X2-rated ceramic capacitors for a capacitance to ground $C_g = 20$ nF.

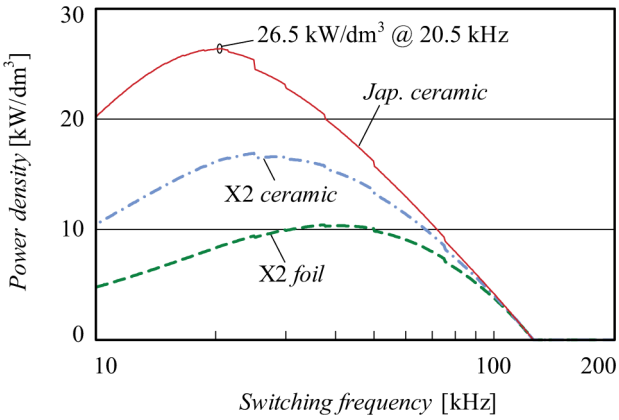

Fig. 19. Power density limits for three different capacitor technologies as a function of the switching frequency considering only the EMC for a 5-kVA SMC.

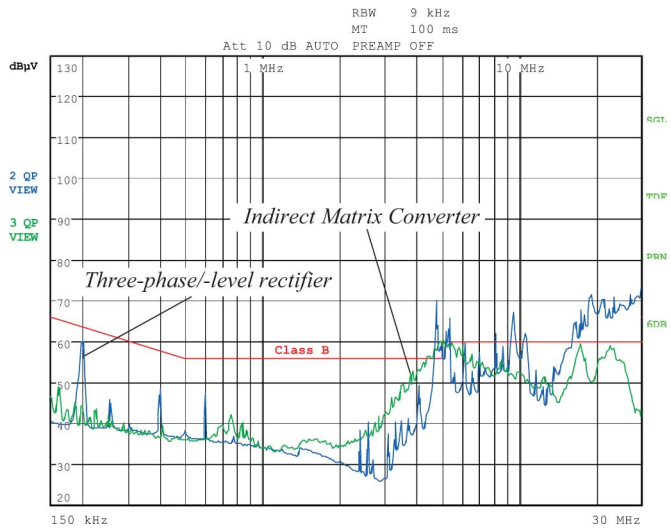

Fig. 20. Measured CM and DM CEs for the two converters under analysis.

frequencies in Fig. 18 is a result of the lower required output CM choke, resulting in the increase of the input sided components. An increased total volume is seen at 150 kHz due to the CE requirements and the necessity of filtering low-order switching frequency harmonics. Furthermore, the total volumes of the DM and CM filters for the SMC implemented and analyzed in [17] are shown as the implemented filters. It is observed that the DM filter is approximately 29% larger than the prediction and that the CM filter is 14% smaller. These figures are within the expected variation range, since many simplifying assumptions have been taken.

Taking the results shown in Fig. 18, it is possible to derive power density limit curves as a function of the switching frequency. This is done in Fig. 19 for three different capacitor technologies. Since the power semiconductor losses reduce the achievable power density for higher switching frequencies, it is seen that a power density limit of 26.5 kW/liter is achieved with ceramic capacitors rated for the Japanese mains at a switching frequency of 20 kHz. This frequency is around 26–41 kHz for the other capacitor technologies, but at much lower power densities. This shows the importance of the improvement of passive components technology for increasing power density.

Conducted emissions (QP) measurements, according to CISPR 22 have been performed in order to experimentally verify the design for each of the converters under analysis. These measurements are shown in Fig. 20. Both results are obtained in open systems, where no special shield was used. This explains for the worsening of the performance for higher frequencies. Nevertheless, the design procedure for the filters prove efficient since the components are designed for the range close to the switching frequency.

VI. Vienna Rectifier Power Density Limits

The same type of calculations are made for a 10-kW Vienna rectifier considering the empirically approximated voltage spectra envelopes, and the CEs requirements for CISPR 22 Class B and design procedures presented previously.

Equally distributing the CM inductors and Y-capacitors among the filter stages leads to the required impedance for inductors $L_{CM,i}$ with $i = 1, \ldots, 3$, as shown in Fig. 21. The

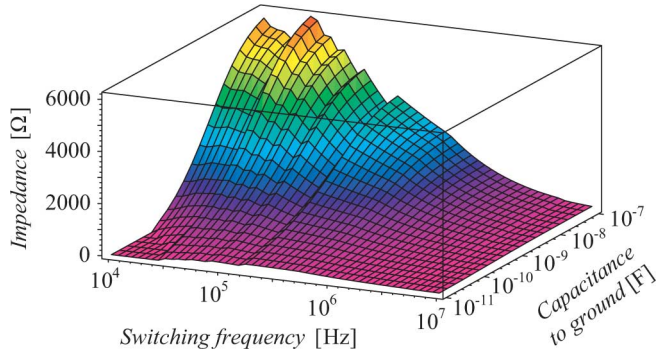

Fig. 21. Required impedance for the CM inductors $L_{CM,i}$, with $i = 1, \ldots, 3$, if these are equally distributed among three *LC* stages.

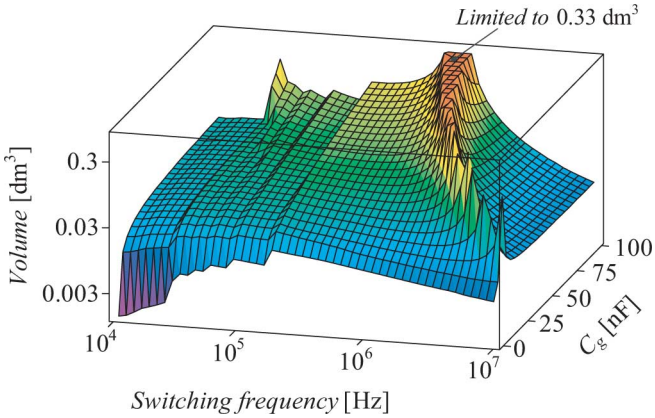

Fig. 22. CM filter volume in dependency of total capacitance to PE C_g and switching frequency f_s.

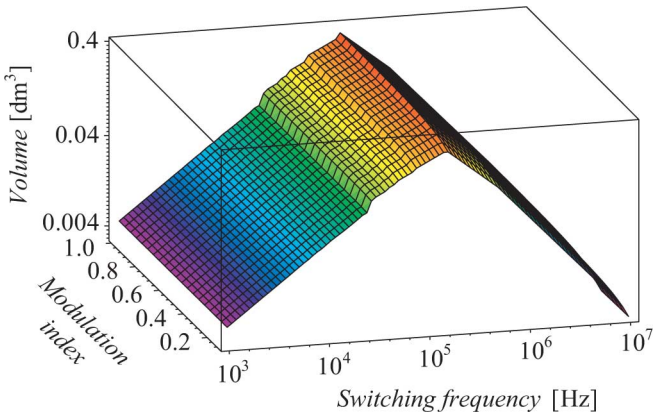

Fig. 23. Estimated volume for the DM filter components for the 10 kW Vienna rectifier excluding the input DM capacitors $C_{DM,1}$ and the boost inductors L_{boost}.

required impedances are highly dependent on the capacitance to PE C_g. The characteristic of the curve changes completely for capacitance values higher or lower than some nanofarads. If C_g is much lower than 1 nF, then the impedance increases up to 150 kHz and then decreases. For high values of capacitance, the required impedances are very high for low switching frequencies and falls rapidly with higher frequencies. These characteristics show the importance of the correct estimation of the stray capacitances in a PWM converter. However, the first inductor is typically subjected to higher HF voltage amplitudes. This leads to larger $L_{CM,1}$, so that the second and third inductors can be smaller in volume and, most of the time, in impedance as well.

Following the aforementioned considerations lead to the total volume of the CM filter components, as shown in Fig. 22. For capacitances C_g lower than approximately 20 nF, the volume of the CM filter increases for switching frequencies up to 150 kHz. This is expected, since the order of the harmonic components that are to be filtered decrease with f_s, and at 150 kHz, the first harmonic would have to be filtered. It is seen that small value of capacitance to PE strongly helps to reduce the CM emissions. Another observation is made on the peak that goes from 10 to 1 MHz with increasing capacitance C_g value. This peak is due to a resonance between the boost inductors and C_g, which is responsible for the strong increase in the voltage across the first CM inductor $L_{CM,1}$ and consequent enlargement of this inductor.

The total volume of the differential mode filter is shown in Fig. 23 as a function of the converter's modulation index M and of the switching frequency f_s. The maximum volume is found at 150 kHz, which is the frequency where the CE regulations start, so that if the switching frequency is equal to 150 kHz, the first harmonic of the switching frequency must be filtered. For frequencies beyond 150 kHz, the volume of the filter components starts to decrease with a ratio of approximately -20 dB/decade. It is observed that, in order to achieve the same volume as for a 20 kHz switching frequency, the switching frequency must be made higher than approximately 800 kHz. It is also observed in Fig. 23 that the volume of the filters does not significantly changes with modulation index.

For the designed rectifier [32], a custom designed power module is employed. For the forced air cooling system, again it is considered CSPI $= 25\,\mathrm{W/K^{-1}\,dm^{-3}}$. While for the water-cooled system, the dimensions as in [33] are employed. The semiconductor power losses are computed considering the set of semiconductors: CoolMOS 600 V, 47 A C3, and Cree SiC Schottky diodes 600 V, 6 A. The analysis is performed for junction temperatures up to 125 °C and ambient temperature of 45 °C. A total capacitance to ground of $C_g = 2$ nF is considered. The DM capacitors are X2-rated ceramics. The estimated volumes are depicted in Fig. 24(a). It is seen that the DM filter (mainly the boost inductors) dominates the volume for low frequencies, whereas the CM is larger for higher switching frequencies. The increase in the switching losses is responsible for the large increase of the cooling system at high frequencies until it limits the feasibility of the rectifier for requiring negative thermal resistances. Fig. 24(b) presents the achievable power densities, for not just the EMC filters and cooling system but also for a water-cooled system. A water-cooled system is capable of further increasing the power density for high switching frequencies. For an air-cooled system, the higher power density is calculated as 39.9 kW/dm^3 for f_s 540 kHz.

For this system, the implementation presented in [26] has been carried out, and the final volumes for the EMC filters are also included in Fig. 24. A comparison with the predicted

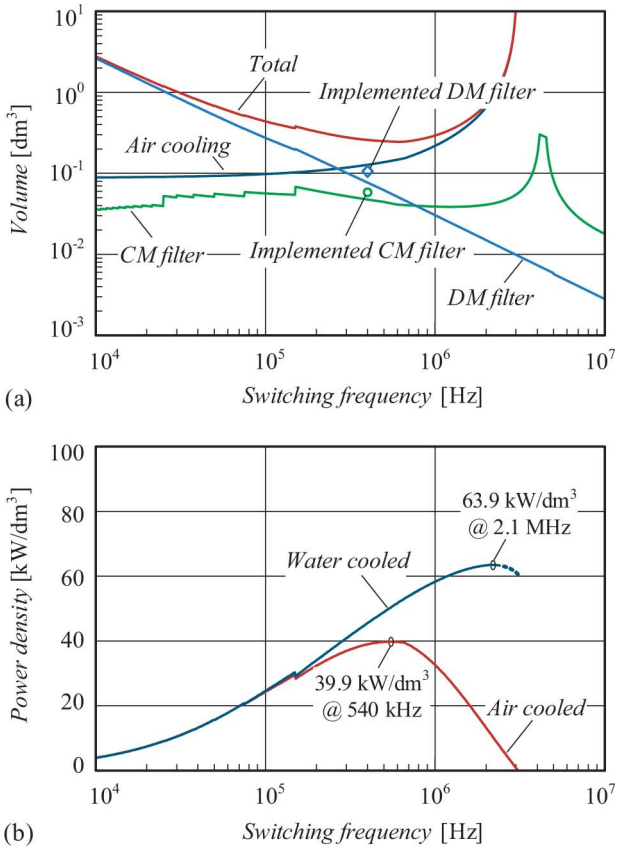

Fig. 24. EMC filters and cooling devices estimated. (a) Volume, with the final volume for the designed filters shown. (b) Power density in dependence of the switching frequency. The influence of the volumes of the CM and DM filter components, including the boost inductors and of the forced air cooling devices (fans and heat sink) is observed in the curves. The curves are generated for a total capacitance to ground of 2 nF. A curve for a possible water-cooled system is added.

volumes can be made leading to an error of 37% for the DM filter components and 22% for the CM ones. This is considered within the expected range arising from all simplifications made in the prediction procedure. Interesting information is that the final boxed volume of the complete filter is approximately 2.4 times larger than the sum of all individual components, meaning that interconnections, air, and PCB account for nearly 60% of the employed space. This leaves room for improvements through further research on intercomponents coupling reduction, materials, and packaging.

VII. Conclusion

This paper has discussed the increase in power density in power electronics systems as an important FOM for such systems. Driven by the importance of this characteristic, the impact of the EMC filters in the achievable power density of two types of three-phase PWM converters has been studied for converters in the range of 5–10 kW.

A design procedure for the EMC filters has been proposed in order to fulfill CISPR 11 Class B requirements related to CEs for two types of PWM converters, an SMC and a three-level/-phase six-switch boost-type rectifier. The design procedure is explained, where a volumetric optimization is carried out taking into consideration different aspects related to the subject, such as electrical safety, power factor, and damping of resonances. The presented procedure allows for the analytical calculation of the total filter volume as a function of the rated power and switching frequency; therefore, helping in the early determination of the optimum switching frequency for a given rectifier specification. A discussion about the limits of power density for the considered three-phase PWM converters for state-of-the-art power semiconductors has been done, and optimum switching frequency has been identified for an optimized forced air-cooled system and for an water-cooled three-level/-phase six-switch boost-type rectifier.

The experimental verification of the proposed filter design procedure is limited to two examples, one for each PWM converter. A total error in the volume prediction of 37% (VR)/29% (SMC) for the DM filter components and 22% (VR)/14% (SMC) for the CM ones has been observed. This is considered within the expected range arising from all simplifications made in the prediction procedure.

The performed study shows the importance of optimizing the construction of power electronics systems and highlights some important points for the further increase in power density. Research efforts are required in the fields of magnetic materials, capacitors technology, packaging, and integration of the components, while the effects of the 3D geometries must be considered in order not to influence filtering performance.

References

[1] H. Ohashi, "Possibility of power electronics paradigm shift with wide band gap semiconductors," *Mater. Sci. Forum*, vol. 457–460, no. 1, pp. 21–26, 2004.

[2] H. Ohashi, "Power electronics innovation with next generation advanced power devices," in *Proc. Int. Telecommun. Energy Conf.*, 2003, pp. 9–13.

[3] A. Mertens, "Innovationen und trends der leistungelektronik," (in German), *VDE ETG-Mitgliederinformation.*, vol. 1, pp. 7–12, Jan. 2007.

[4] F. C. Lee and P. Barbosa, "The state-of-the-art power electronics technologies and future trends," in *Proc. IEEE PES Transmiss. Distrib. Conf. Expo.*, 2001, vol. 2, pp. 1188–1193.

[5] S. Round, F. Schafmeister, M. Heldwein, E. Pereira, L. Serpa, and J. Kolar, "Comparison of performance and realization effort of a very sparse matrix converter to a voltage DC link PWM inverter with active front end," presented at the Int. Power Electron. Conf., Niigata, Japan, 2005.

[6] S. D. Round, P. Karutz, M. L. Heldwein, and J. W. Kolar, "Towards a 30 kW/liter, three-phase unity power factor rectifier," presented at the Power Convers. Conf., Nagoya, Japan, 2007.

[7] P. W. Wheeler, J. Rodriguez, J. C. Clare, L. Empringham, and A. Weinstein, "Matrix converters: A technology review," *IEEE Trans. Ind. Electron.*, vol. 49, no. 2, pp. 276–288, Apr. 2002.

[8] G. Gong, M. L. Heldwein, U. Drofenik, J. Minibock, K. Mino, and J. W. Kolar, "Comparative evaluation of three-phase high-power-factor AC–DC converter concepts for application in future more electric aircraft," *IEEE Trans. Ind. Electron.*, vol. 52, no. 3, pp. 727–737, Jun. 2005.

[9] L. A. Saunders, G. L. Skibinski, S. T. Evon, and D. L. Kempkes, "Riding the reflected wave IGBT drive technology demands new motor and cable considerations," in *Proc. IEEE Petroleum Chem. Ind. Conf.*, 1996, pp. 75–84.

[10] J. W. Kolar and H. Ertl, "Status of the techniques of three-phase rectifier systems with low effects on the mains," in *Proc. IEEE Int. Telecommun. Energy Conf.*, 1999, Paper no. 14-1.

[11] B. Singh, B. N. Singh, A. Chandra, K. Al Haddad, A. Pandey, and D. P. Kothari, "A review of three-phase improved power quality AC–DC converters," *IEEE Trans. Ind. Electron.*, vol. 51, no. 3, pp. 641–660, Jun. 2004.

[12] E. Zhong and T. A. Lipo, "Improvements in EMC performance of inverter-fed motor drives," *IEEE Trans. Ind. Appl.*, vol. 31, no. 6, pp. 1247–1256, Nov./Dec. 1995.
[13] Y. Zhao, Y. Li, and T. A. Lipo, "Force commutated three level boost type rectifier," in *Proc. IEEE Ind. Appl. Soc. Annu. Meeting*, 1993, vol. 2, pp. 771–777.
[14] J. W. Kolar and F. C. Zach, "A novel three-phase utility interface minimizing line current harmonics of high-power telecommunications rectifier modules," *IEEE Trans. Ind. Electron.*, vol. 44, no. 4, pp. 456–467, Aug. 1997.
[15] N. Backman and R. Rojas, "Modern circuit topology enables compact power factor corrected three-phase rectifier module," in *Proc. Telecommun. Energy Conf., 2002, INTELEC. 24th Annu. Int.*, pp. 107–114.
[16] YASKAWA, "Yaskawa's variable speed AC motor control—First comercially available matrix converter drive," *Yaskawa Tech. Rev.*, vol. 69, no. 2, pp. 75–78, 2005.
[17] T. Friedli, M. L. Heldwein, F. Giezendanner, and J. W. Kolar, "A high efficiency indirect matrix converter utilizing RB-IGBTs," in *Proc. IEEE Power Electron. Spec. Conf.*, 2006, pp. 1–7.
[18] K. Iimori, K. Shinohara, O. Tarumi, Z. Fu, and M. Muroya, "New current-controlled PWM rectifier-voltage source inverter without DC link components," in *Proc. Power Convers. Conf.*, Nagaoka, Japan, 1997, pp. 783–786.
[19] L. Wei and T. A. Lipo, "A novel matrix converter topology with simple commutation," in *Proc. Ind. Appl. Conf.*, 2001, vol. 3, pp. 1749–1754.
[20] P. Zwimpfer and H. Stemmler, "Modulation and realization of a novel two-stage matrix converter," presented at the Brazilian Power Electron. Conf., Florianopolis, Brazil, 2001.
[21] J.-I. Itoh, I. Sato, A. Odaka, H. Ohguchi, H. Kodachi, and N. Eguchi, "A novel approach to practical matrix converter motor drive system with reverse blocking IGBT," *IEEE Trans. Power Electron.*, vol. 20, no. 6, pp. 1356–1363, Mar. 2005.
[22] J. W. Kolar, F. Schafmeister, S. D. Round, and H. Ertl, "Novel three-phase AC–AC sparse matrix converters," *IEEE Trans. Power Electron.*, vol. 22, no. 5, pp. 1649–1661, Sep. 2007.
[23] *Vitroperm 500 F—Vitrovac 6030 F—Tape Wound Cores in Power Transformers for Switch Mode Power Supplies*, Vacuumschmelze (VAC) GmbH and Company, Hanau, Germany, 2003.
[24] Vacuumschmelze (VAC) GmbH and Company. (2004). Nanocrystalline Vitroperm EMC Components. Hanau, Germany. [Online]. Available: http://www.vacuumschmelze.com/dynamic/docroot/medialib/documents/broschueren/kbbrosch/PKB_EMV_E.pdf
[25] Murata, "Chip monolithic ceramic capacitors," 2007.
[26] M. L. Heldwein and J. W. Kolar, "Design of minimum volume EMC input filters for an ultra compact three-phase PWM rectifier," presented at the Brazilian Power Electron. Conf. (COBEP 2007), Blumenau, Brazil, [CD-ROM].
[27] Evox-Rifa, "RFI capacitors for the AC line (X and Y capacitors)," 2007.
[28] L. Ran, S. Gokani, J. Clare, K. J. Bradley, and C. Christopoulos, "Conducted electromagnetic emissions in induction motor drive systems, Part I: Time domain analysis and identification of dominant modes," *IEEE Trans. Power Electron.*, vol. 13, no. 4, pp. 757–767, Jul. 1998.
[29] *Industrial, Scientific and Medical (ISM) Radio-Frequency Equipment—Electromagnetic Disturbance Characteristics—Limits and Methods of Measurement—Publication 11*, IEC International Special Committee on Radio Interference, CISPR Standard, 2004.
[30] T. Friedli, S. D. Round, and J. W. Kolar, "A 100 kHz SiC sparse matrix converter," in *Proc. IEEE Power Electron. Spec. Conf.*, 2007, pp. 2148–2154.
[31] U. Drofenik and J. W. Kolar, "Analyzing the theoretical limits of forced air-cooling by employing advanced composite materials with thermal conductivities >400W/mK," in *Proc. IEEE Conf. Integr. Power Syst.*, Naples, Italy, 2006, pp. 323–328.
[32] P. Karutz, S. D. Round, M. L. Heldwein, and J. W. Kolar, "Ultra compact three-phase PWM rectifier," in *Proc. Appl. Power Electron. Conf.*, 2007, pp. 816–822.
[33] U. Drofenik, G. Laimer, and J. W. Kolar, "Pump characteristic based optimization of a direct water cooling system for a 10-kW/500-kHz vienna rectifier," *IEEE Trans. Power Electron.*, vol. 20, no. 3, pp. 704–714, May 2005.

Marcelo Lobo Heldwein (M'99) received the B.S. and M.S. degrees in electrical engineering from the Federal University of Santa Catarina (UFCS), Florianópolis, Brazil, in 1997 and 1999, respectively, and the Ph.D. degree from the Swiss Federal Institute of Technology (ETH Zurich), Zurich, Switzerland, in 2007.

He is currently working as a Postdoctoral Fellow at the Power Electronics Institute (INEP), UFSC, under the PRODOC/CAPES program. From 1999 to 2001, he was a Research Assistant with the Power Electronics Institute, Federal University of Santa Catarina. From 2001 to 2003, he was an Electrical Design Engineer with Emerson Energy Systems, in São José dos Campos, Brazil and in Stockholm, Sweden. His research interests include power factor correction techniques, static power converters, and electromagnetic compatibility.

Dr. Heldwein is currently a member of the Brazilian Power Electronic Society (SOBRAEP).

Johann W. Kolar (M'89–SM'04) received the Ph.D. degree (*summa cum laude/promotio sub auspiciis praesidentis rei publicae*) from Vienna University of Technology, Vienna, Austria, in 1998.

Since 1984, he has been an Independent International Consultant in close collaboration with Vienna University of Technology, where he is engaged in the fields of power electronics, industrial electronics, and high-performance drives. Since February 2001, he has been a Professor and the Head of the Power Electronic Systems Laboratory, Swiss Federal Institute of Technology (ETH) Zurich, Zurich, Switzerland. He has proposed numerous novel pulsewidth modulation (PWM) converter topologies, and modulation and control concepts, e.g., the VIENNA rectifier and the three-phase ac–ac sparse matrix converter. He has authored or coauthored over 250 scientific papers published in international journals and conference proceedings, and has filed more than 70 patents. Since 2002, he has been an Associate Editor of the *Journal of Power Electronics* of the Korean Institute of Power Electronics and a member of the Editorial Advisory Board of the *Institute of Electrical Engineers of Japan (IEEJ) Transactions on Electrical and Electronic Engineering*. His current research interests include ac–ac and ac–dc converter topologies with low effects on the mains, e.g., for power supply of telecommunication systems, more-electric-aircraft and distributed power systems in connection with fuel cells, realization of ultracompact intelligent converter modules employing latest power semiconductor technology (SiC), novel concepts for cooling and electromagnetic interference (EMI) filtering, multidomain/multiscale modeling and simulation, pulsed power, bearingless motors, and power microelectromechanical systems (MEMS).

Prof. Kolar is a member of the IEEJ and the Technical Program Committees of numerous international conferences in the field (e.g., Director of the Power Quality Branch of the International Conference on Power Conversion and Intelligent Motion). From 1997 to 2000, he was an Associate Editor of the IEEE TRANSACTIONS ON INDUSTRIAL ELECTRONICS. Since 2001, he has been an Associate Editor of the IEEE TRANSACTIONS ON POWER ELECTRONICS. He has received the Best Transactions Paper Award of the IEEE Industrial Electronics Society in 2005. He also received an Erskine Fellowship from the University of Canterbury, New Zealand, in 2003.